

A 3D Discrete Damage Modeling Methodology for Abaqus for Fatigue Damage Evaluation in Bolted Composite Joints

Eugene Fang¹, Jim Lua¹, Ling Liu¹, Michael Stuebner¹

Michael Swindeman² and Endel Iarve²

¹Global Engineering and Materials, Inc., 1 Airport Place, Suite 1, Princeton, NJ 08540, USA

²University of Dayton Research Institute, 300 College Park Avenue, Dayton, OH 45469-0168

Abstract: A discrete multi-mode damage initiation, propagation, and interaction tool is implemented within Abaqus' implicit solver for residual strength and life prediction of bolted joints with a given initial damage resulting from the fabrication and installation process. A discrete crack network model (DCN) for damage progression prediction has been developed by combining mesh independent matrix cracking with cohesive zone delamination models at the ply interfaces. A regularized X-FEM (Rx-FEM) framework maintaining the distribution of the Gauss integration points without element slicing has been utilized for implementation of the solution module for residual strength prediction under monotonic loading. A Virtual Crack Closure Technique based conventional X-FEM with cohesive spring bond for the energy release rate computation has been implemented in the DCN toolkit for fatigue loading. The fracture parameters are extracted at an evolving crack front within a mesh independent framework and used to perform the subsequent fatigue life prediction through a concurrent analysis procedure. To capture the pre-tension and contact in a bolted composite system under bearing and bypass loading, an overlay element approach is also implemented to couple our user-defined elements with Abaqus elements to enhance the solution capability and applicability. Verification and validation study are performed using a set of benchmark problems at the coupon and subcomponent level.

Keywords: Composite Bolted Joint, Fastener Holes, Matrix Cracking, Delamination, Extended Finite Element Method (X-FEM), Regularized X-FEM, Fatigue and Fracture, Abaqus

1. Introduction

Bolted joints are the most common form of joints in composite aircraft structure. Such joints often become the limiting factor for structural efficiency and load-carrying capability. In comparison with adhesively bonded joints, joining by mechanical fasteners offers several advantages: no special surface treatment; capable to join thick structures; and easy access to the interior for inspection and repair purposes. However, the stress concentration developed around the holes can severely reduce the strength and fatigue life of the structure in bolted composite structures. Despite the extensive use of composite bolted joints in primary structures, the fatigue behavior of

composites has been long neglected in the aerospace applications due to relatively limited service hours of high performance fixed wing aircraft and general overdesign of composite part, which are operating at the load levels significantly below fatigue damage thresholds. This paradigm is rapidly changing under the influence of ever increasing performance and cost efficiency requirements. Consequently the computational capabilities in the area of fatigue life prediction of composites elements and structures are rather limited as compared to those available for static analysis. An Abaqus toolkit proposed in the present paper is developed to address this need. We aim at reducing the cost and design cycle and including the matrix cracking and delamination initiation, propagation, and interaction to capture the failure sequence, damage pattern, and predict the residual strength and life of a composite bolted joint system in the presence of contact and plastic deformation in the fastener.

Delamination damage mode is of great practical importance in bolted composite joints. However, it cannot be isolated from matrix cracking. Matrix cracks are usually the initiation sites of delamination. Depending upon the layup and loading profile, several scenarios directly influencing the damage tolerance assessment are possible: matrix cracking can temporarily arrest the delamination; it can divert the delamination to a different interface; or it may cause an avalanche of multiple delaminations through the thickness of the part. Given the strong coupling effect between matrix cracking and delamination, it is necessary for any high-fidelity analysis model to include a discrete matrix and delamination crack network for the residual strength and life prediction of laminated composites.

A significant body of research was devoted to the development of comprehensive damage mechanics models to account for all modes of in-plane failure in composite laminates. These approaches were generally successful in predicting the softening behavior in laminates due to matrix crack accumulation under uniform loading conditions. The value of the continuum damage models is the ability to describe the stiffness response of a laminate containing significant amounts of matrix damage, which cannot be accomplished by explicit crack modeling. The drawback of these models is their inability to accurately describe the local effects of interaction of various damage modes and local effects of stress redistribution in the damaged area. For instance, directional degradation of the transverse properties of the unidirectional ply in the locations associated with splitting results in a qualitatively incorrect effect on the stress/strain distribution in the vicinity of the hole edge and the splits. Moreover that effect is mesh direction dependent. Additional issues associated with the continuum damage modeling of matrix cracking are the lack of a rational and unique way in defining the stiffness reduction of composite (20%, 50%, or 75%) at a given damage state and the infeasibility to perform the test to measure the stiffness degradation at various damage states and combined loading conditions.

The recently developed extended finite element method (X-FEM) has been proved as an efficient way to simulate the mesh-independent crack propagation problem. Iarve (2003) proposed a regularized X-FEM (Rx-FEM) for mesh independent matrix cracking (MIC) modeling, which did not require any modifications of the element boundaries or integration routines. In this case the step function which describes the crack surface was also represented by the same shape functions as used for displacement approximation, resulting in continuous (regularized) approximate step function. No sub-domain integration strategy is required for a cracked element and a standard

Gauss integration scheme can be used for the element stiffness matrix computation. Both the computational efficiency and numerical accuracy have been verified in [Iarve et al., 2002-2006; Mollenhauer et al., 2006] for laminated composites without or with a hole under monotonic loading. Due to the lack of a sharp crack front definition, a cohesive zone model needs to be used for static and consequently fatigue analysis within the Rx-FEM framework.

Recently Turon et al [2] proposed an approach to link the damage evolution by using cohesive zone models and the Paris law (PL) for fatigue delamination growth. A damage parameter (D) is introduced by taking the ratio of the damaged area with the total cohesive zone size. An evolution of D (i.e. dD/dN) is computed directly from the dA/dN determined from the experimentally measured DCB and ENF tests. Two issues associated with this approach are: 1) the definition of a delamination front and computation of ΔG along the front using the cohesive model; and 2) direct use of the measured Paris parameters from DCB/ENF tests to compute the damage evolution dD/dN without any calibration. These difficulties arise from the principle differences in representing the crack front in the fracture mechanics framework (FMF) of the PL and that in the cohesive zone model. Namely, in FMF the crack tip separates the undamaged portion of the interface and its cracked portion and represents a point in the two-dimensional case. The PL defines the propagation of the crack tip as a function of cycles and the crack tip driving force. On the other hand it is the definition of the crack tip, which is not present in the cohesive zone model and requires reinterpretation of the PL in the presence of the process zone at the crack tip.

While the fundamental work on development and validation of fatigue cohesive zone models will continue we will implement a more conventional Virtual Crack Closure Technique (VCCT) based fatigue framework first. We will retain the mathematical description of a sharp crack front by using the X-FEM without its regularization for the simulation of fatigue crack growth. The fatigue crack growth driving parameter (ΔG) will be directly computed along a moving delamination front via phantom paired elements coupled with the injection of discrete springs for ΔG extraction using the VCCT approach. Two key components of the Abaqus toolkit for the residual strength and life prediction of bolted composite joints are discussed next along with their implementation via the UEL and UEXTERNALDB: 1) regularized X-FEM (Rx-FEM) for mesh independent discrete crack network (DCN) characterization under monotonic loading; and 2) phantom-paired X-FEM for mesh independent DCN characterization under fatigue loading. Both the applicability and accuracy of both the monotonic and fatigue solution modules are demonstrated via a set of example problems.

2. Regularized extended finite element method (Rx-FEM)

Consider a domain Ω shown in Figure 1, with a prescribed traction \bar{t} on Γ_t and displacement on Γ_u . A general form of the displacement field can be written as

$$\mathbf{u}(\mathbf{x}) = \sum_{i \in I} X_i(\mathbf{x}) \mathbf{u}_i \quad (1)$$

where $\mathbf{u}(\mathbf{x})$ is the displacement at position \mathbf{x} , $X_i(\mathbf{x})$ are the shape functions which provide a partition of unity on this domain and \mathbf{u}_i are the displacement approximation coefficients. In Eq. (1), index i changes from 1 to the total number of partition of unity functions denoted by set I .

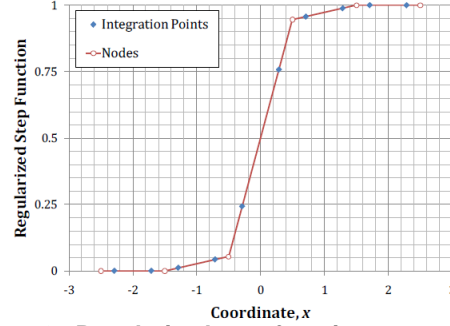
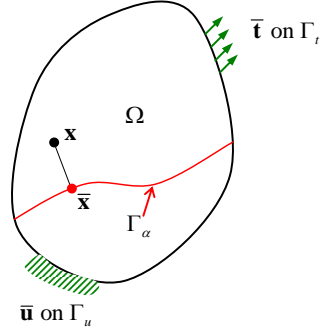


Figure 1. A problem domain with a crack. Figure 2. Regularized step function example [3].

If there exists a discontinuity in the domain denoted by Γ_α defined by a signed distance function $f_\alpha(\mathbf{x})$ computed based on the relative position between the crack surface Γ_α and point \mathbf{x} , i.e.,

$$f_\alpha(\mathbf{x}) = \text{sign}[\mathbf{n}(\bar{\mathbf{x}})(\mathbf{x} - \bar{\mathbf{x}})] \min_{\bar{\mathbf{x}} \in \Gamma_\alpha} \|\mathbf{x} - \bar{\mathbf{x}}\| \quad (2)$$

where $\mathbf{n}(\bar{\mathbf{x}})$ is the unit normal vector to the surface Γ_α at point $\bar{\mathbf{x}}$. In this case the displacement approximation can be written as

$$\mathbf{u}(\mathbf{x}) = \sum_{i \in I/J} X_i(\mathbf{x})\mathbf{u}_i + H(f_\alpha(\mathbf{x})) \sum_{j \in J} X_j(\mathbf{x})\mathbf{u}_j^{(1)} + [1 - H(f_\alpha(\mathbf{x}))] \sum_{j \in J} X_j(\mathbf{x})\mathbf{u}_j^{(2)} \quad (3)$$

where the Heaviside function used in Eq. (3) is defined as

$$H(x) = \begin{cases} +1 & x \geq 0 \\ 0 & x < 0 \end{cases} \quad (4)$$

The key idea of the Rx-FEM is to replace the conventional step function, which is discontinuous, by a regularized step function $\tilde{H}(\mathbf{x})$ that is continuous across the crack surface Γ_α as shown in Fig. 2. In our method the continuous or regularized step function is approximated by using the same shape functions as the displacement approximation. Similar to the standard X-FEM method, the final stiffness matrix takes the form as

$$\int_{\Omega} \begin{bmatrix} \mathbf{X}^T \mathbf{D} \mathbf{X} \tilde{H} & 0 & \mathbf{X}^T \mathbf{D} \mathbf{X} \tilde{H} \\ 0 & \mathbf{X}^T \mathbf{D} \mathbf{X} (1 - \tilde{H}) & \mathbf{X}^T \mathbf{D} \mathbf{X} (1 - \tilde{H}) \\ \text{sym} & \text{sym} & \mathbf{X}^T \mathbf{D} \mathbf{X} \end{bmatrix} d\Omega \begin{Bmatrix} \mathbf{u}^{(1)} \\ \mathbf{u}^{(2)} \\ \mathbf{u}^{(3)} \end{Bmatrix} = \begin{Bmatrix} \mathbf{t}^{(1)} \\ \mathbf{t}^{(2)} \\ \mathbf{t}^{(3)} \end{Bmatrix} \quad (5)$$

where $\mathbf{t}^{(1)}$, $\mathbf{t}^{(2)}$ and $\mathbf{t}^{(3)}$ are the equivalent force vector corresponding to the associated degree of freedoms of $\mathbf{u}^{(1)}$, $\mathbf{u}^{(2)}$, and $\mathbf{u}^{(3)}$. They can be written as

$$\begin{Bmatrix} \mathbf{t}^{(1)} \\ \mathbf{t}^{(2)} \\ \mathbf{t}^{(3)} \end{Bmatrix} = \int_{\Gamma_t} \begin{Bmatrix} \mathbf{X}^T \tilde{H} \\ \mathbf{X}^T (1 - \tilde{H}) \\ \mathbf{X}^T \end{Bmatrix} \bar{\mathbf{t}} d\Gamma \quad (6)$$

The Rx-FEM [1] is originally incorporated into the stand-alone finite element code B-Spline Analysis Method software (BSAM). Despite that the stand alone code BSAM developed by UDRI has been validated by numerous tests performed by Air Force, the lack of integration and compatibility with existing commercial finite element solvers such as Abaqus limits its viability for commercialization. In addition, given the complexity of the bolted joint associated with the contact, plastic deformation in the fastener, hole wearing, hole edge crushing, and micro-buckling near the compressive loading zone, it is rational to be combined with Abaqus’ existing capability through the integration of key BSAM solution modules with Abaqus’ user-defined subroutines. The UEL is for the definition of the element stiffness matrix and its residual force vector while UEXTERNALDB is used to handle the external memory database and controls its solution process.

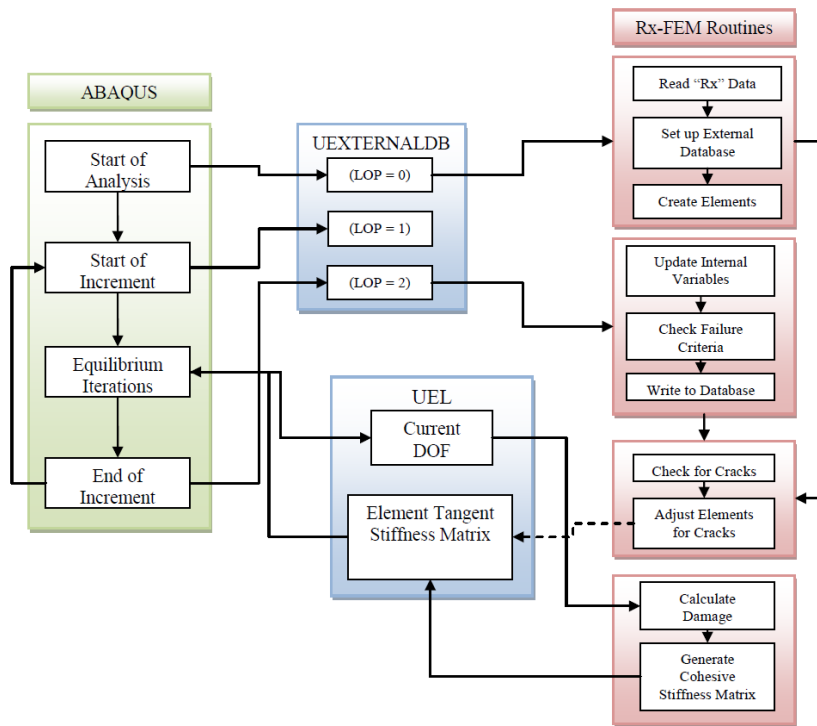


Figure 3. Flowchart of the implementation of Rx-FEM within Abaqus.

A general block diagram for the implementation of Rx-FEM in Abaqus is shown in Fig. 3. The entire implementation is accomplished via two different levels: increment level and element level. At the increment level, the subroutine UEXTERNALDB provides a parameter LOP to indicate the solution status: beginning of the analysis (LOP=0), beginning of the increment (LOP=1), end of the increment (LOP=2), and the end of the analysis (LOP=3). At the beginning of the analysis, Rx-FEM modules will read in the model information, set up the database and treat the initial cracked elements. At the end of every increment, Rx-FEM modules will be called to check the failure criteria to determine the newly cracked elements. Some selected results are also written into the external database.

The subroutine UEL is called for every user-defined element at every iteration. Firstly, the current element is checked to see if it is cracked or not. Then relevant subroutines in Rx-FEM modules are called in UEL to obtain the stiffness matrix and RHS. For a cracked element, a cohesive interaction is applied and its additional contribution to both the stiffness matrix and residual force is determined within the cohesive module (see Fig. 4). In the stand-alone program BSAM, additional nodes or degrees of freedom can be introduced for crack generation. However Abaqus does not support the change of degrees of freedom (DoFs) during the solution process. To circumvent this difficulty, each node is prescribed at the very beginning to have 6 DoFs, where the first 3 DoFs are the standard displacement DoFs and the 4~6 DoFs are the “phantom” displacement variables despite if the element is intact or cracked. Once the element is detected to be cracked, these “phantom” DoFs will be activated to represent the discontinuous displacement field. If the element is intact, the “phantom” DoFs are not activated and a special treatment of the stiffness matrix is applied to suppress the numerical singularity. Thus, it is necessary to map the stiffness matrix and residual force vector from Rx-FEM modules into the element matrix properly within the UEL.

To correctly characterize the energy dissipation during the crack propagation, a cohesive interaction module shown in Fig. 4 is implemented based on the mixed cohesive law proposed by Camanho and Davila (2002). The cohesive interaction is defined via Abaqus’ UEL where both the stiffness and the load vector are computed.

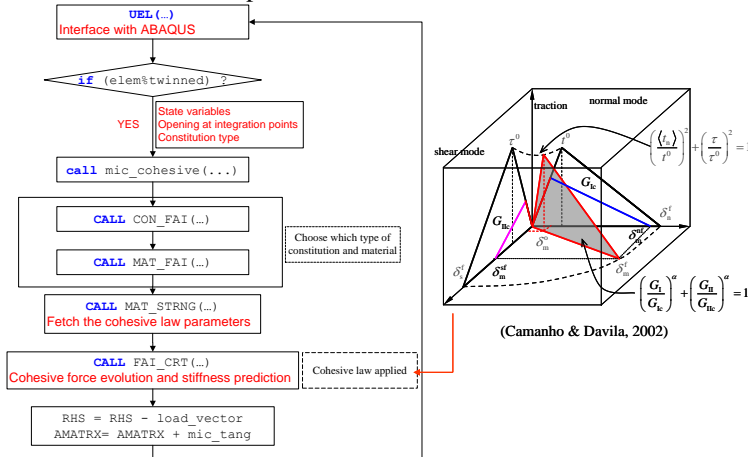


Figure 4. Implementation of cohesive interaction

3. Phantom paired X-FEM fatigue analysis module

3.1 Discrete crack representation with phantom pair elements

In the above section, the Rx-FEM has been implemented in Abaqus to simulate both the matrix crack initiation and propagation under the monotonic loading. Due to a smearing process used in the crack front definition, only cohesive zone based crack opening mechanisms can be implemented at present. To implement fracture mechanics based fatigue crack growth model, a phantom paired X-FEM is implemented to retain the sharp crack front for its fatigue crack growth simulation. A phantom-paired X-FEM is used to correctly characterize the kinematics of a cracked element while an injected spring constraint is used to extract the range of the strain energy release rate (ΔG) along the mesh independent crack front using VCCT. Here the spring is introduced automatically at a crack front which is located at an intersection point between an element edge and the evolving crack front. By constraining the relative displacements to be zero at the crack front using the linear spring, the imposed force can be extracted for the ΔG calculation using VCCT. Similar to the Rx-FEM, the displacement is represented by Eq. (3) and the resulting final stiffness matrix has the same form as Eq. (5). Due to use of the standard Heaviside function in X-FEM for the crack front representation, the discontinuity is denoted as a sharp red plane as shown in Fig. 5. For a cracked element, the combination of the physical nodes (without the prime) with the phantom nodes (with the prime) for the phantom paired elements as shown in Fig. 5 where an arbitrary displacement jump across the red plane can be described.

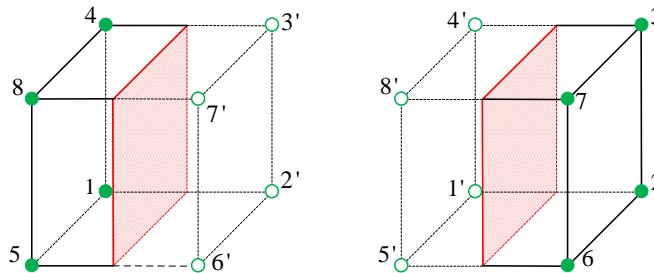


Figure 5. Discontinuity across the crack surface represented by phantom pair element.

Different from a conventional cohesive zone model where both a linear and a softening branch are presented in its constitutive law, a set of linear penalty springs is inserted to extract the traction force at the crack front. Given the mesh independent framework, the penalty springs can be inserted arbitrarily along the crack front without being in conformation to the positions of the existing nodal points. An illustration of the insertion of a penalty spring at the crack front for VCCT calculation is depicted in Fig. 6. To avoid the tip locking and the resulting incorrect crack profile representation as shown in Fig. 7, a virtual extension through a few more elements ahead of a physical crack front is introduced as shown in Fig. 7 to enhance the deformation modes (weak discontinuity) without introducing an unrealistic strong discontinuity. The use of the linear spring model for the detection of a physical crack front and the extraction of the strain energy release rate along its front are given below along with the crack front update based on the computed ΔG and a Paris fatigue crack growth law.

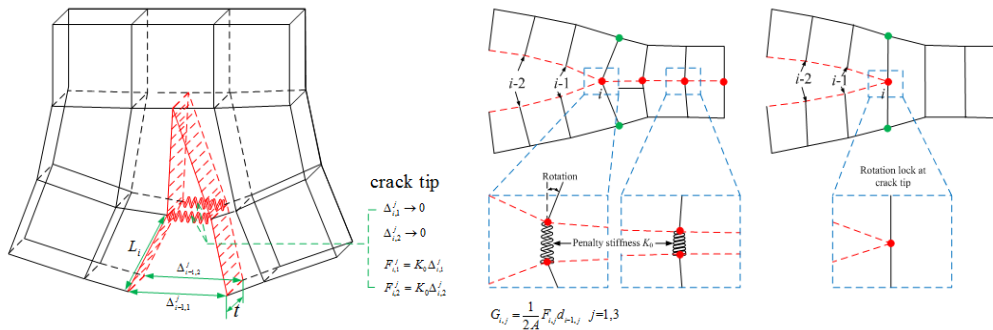


Figure 6. VCCT with phantom pair approach. Figure 7. Virtual extension for release tip locking.

3.2 Discrete spring model for mesh-independent fatigue delamination

A discrete spring model is implemented in both UINTER and UEL for simulating interfacial contact and delamination behavior (see Fig. 8(a)). For any two nodes that form a contact pair, two modes are considered in the spring model: (1) bonded node-pair and (2) debonded node-pair. When the node-pair is in its bonding status, we assume there is a very thin elastic layer that fills the “gap” between these two surfaces. No matter if the contact is in compression (when the nodal separation is positive according to Abaqus convention) or in tension (when the nodal separation is negative), the interaction force (or stress) is evaluated by an elastic relationship. In the UEL-based approach, each node on the slave surface is paired with a node on the master surface and they are linked with a user-defined element, whose internal force (RHS) is calculated via the UEL subroutine with their nodal displacements (U) as input.

The calculation of the energy release rate via VCCT requires two components at a delamination front: (1) internal forces associated with the node of interest residing on the crack front; and (2) relative displacement between the debonded interfaces at a sampling point with a small distance away from the node of interest. As illustrated in Fig. 8 (b), node “O” is the stress sampling point and point “C” is the relative displacement sampling point in the debonded zone. Line segment between “C” and “O” is perpendicular to the local delamination front. And the distance between them is $\sqrt{A_o}$, where A_o is the representative area of node “O”. When a quadrilateral element is used, A_o is the one-fourth of the total area of the element that shares node “O”. Once the sampling stress and relative displacement are extracted, the energy release rate is computed by $G = \sigma_o \delta_c / 2$, where σ_o is the stress at node “O” and the δ_c is the relative displacement at point “C”. After obtaining the energy release rate, the Paris law is applied to compute the delamination front propagation speed. To grow the front there are two things required: (1) select a point to move; (2) compute the move distance and direction. The closest points on the physical delamination front to the nodes on the FE front are selected as the representative points to move. The outward normal direction is taken as the front growth direction as shown in Fig. 9(a). The

attractive character of this approach is that multiple delamination fronts can merge into each other naturally (see Fig. 9(b)).

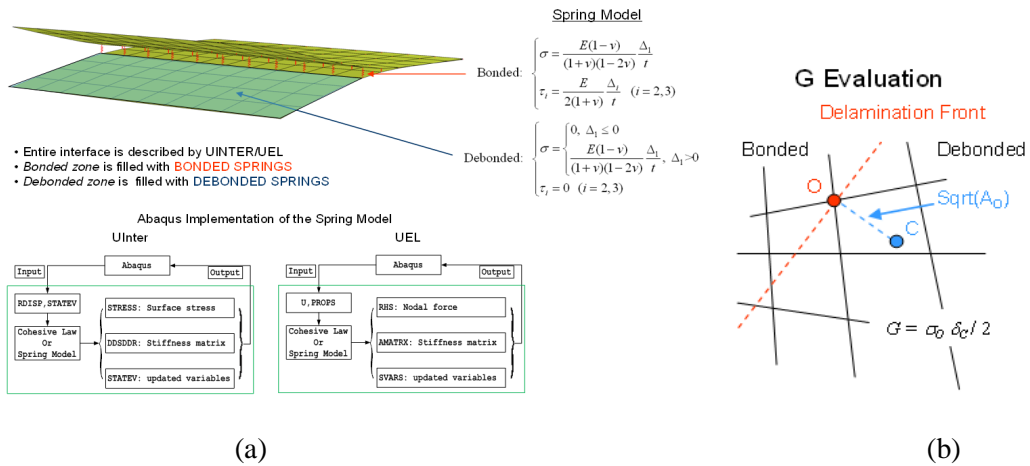


Figure 8. Discrete spring model for fatigue delamination (a) its Abaqus implementation (b) scheme for extraction of energy release rate.

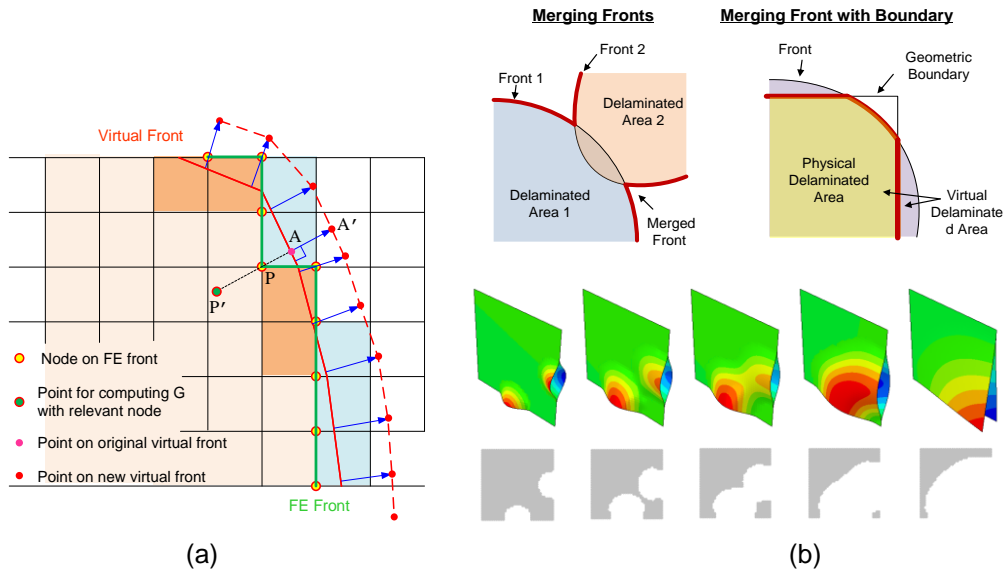


Figure 9. Mesh independent delamination (a) propagation and (b) merge.

4. Example applications and capability demonstrations

After integration of both the Rx-FEM and phantom paired X-FEM solution modules in the DCN toolkit for Abaqus, a set of demonstration examples are selected to explore their applicability and capability in simulation of discrete damage progression and interaction in a laminated composite structure under monotonic and cyclic loading.

4.1 Double cantilever beam

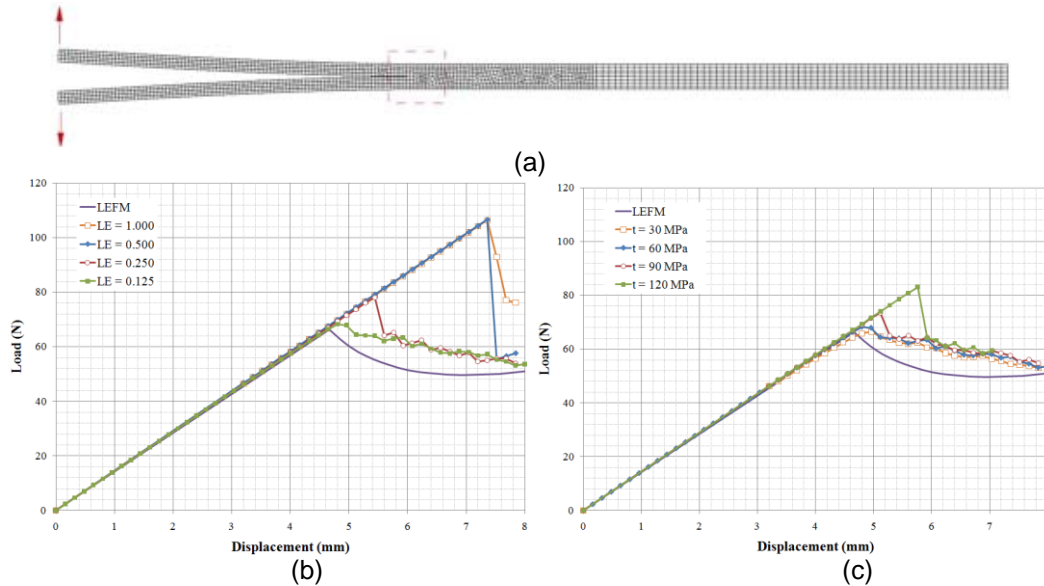


Figure 10. DCB crack propagation simulation: (a) configuration; (b) element size sensitivity analysis; (c) peak strength sensitivity analysis.

Table 1 material and interfacial properties [4]

E_{11} (GPa)	$E_{22} = E_{33}$ (GPa)	$G_{12} = G_{13}$ (GPa)	G_{23} (GPa)
150.0	11.0	6.0	3.7
$\nu_{12} = \nu_{13}$	ν_{23}	G_{Ic} (N/mm)	σ_0 (MPa)
0.25	0.45	0.352	60.0

The first example is a double cantilever beam (DCB). It is often used to verify the cohesive models by monitoring the load-deflection history. The DCB configuration is shown in Fig. 10(a). It is 150 mm long with a 55 mm long pre-existing crack. The height of either arm is 1.98 mm and the width is 20 mm. The material properties are listed in Table 1. Fig.10 (b) shows a comparison between the load-displacement relationship predicted from Rx-FEM and the LEFM solution. Here two different element sizes are used to investigate the mesh size effect on the cohesive model. The predicted cohesive zone length for this Mode-I case is about 1.0 mm. Results at element size l_e

=1.0, 0.5, 0.25 and 0.125 mm are given in Fig. 10 and the use of the refined mesh can predict peak load more precisely. When the mesh is very coarse and is comparable with the cohesive zone length, the predicted peak load is much higher than the convergent solution.

4.2 Laminate plate under tension

This example is to demonstrate the capability of Rx-FEM in simulating the coupled matrix cracking and delamination for a laminated plate subjected a monotonic tension. The failure progression of this quasi-isotropic laminate is investigated using the DCN toolkit. The detailed description of the specimen can be found in Ref. [7]. The specimen is made of IM7/8552 with stacking sequence of the laminates of $[45_m/90_m/-45_m/0_m]_s$ for $m=1, \dots, 8$. In the following simulation the case $m = 4$ is investigated. The numerical simulation includes two cases: (1) considering only three pre-existing cracks within the 45, 90 and -45 ply respectively (see Fig. 11); (2) considering multiple matrix cracks, i.e., the cracks are generated automatically once the crack initiation criteria are satisfied. An initial delamination occurs at the interface between 90/45 plies and finally the delamination will jump into the interface between -45/0 before the complete failure is indicated by the sudden load drop. The stress level for the initiation of the delamination at 90/45 is 380 MPa and the maximum stress before the complete debonding at -45/0 is 502 MPa. All the observed delamination zones initiate from the interactions between matrix cracks and the free edge stress concentration (see Fig.12). The occurrence of matrix cracks will release the stretch stress in plies. The in-ply stress release makes the plies tend to be stress free. However this tendency is prevented by the interaction with the plies which have different fiber directions. The intra-ply interface cohesive traction will rise up to hold on the plies' deformation as the remedy of matrix cracking. The laminate load capacity will be overestimated. Both the failure process and stress levels at different stages agree well with the results in Ref. [7]. And more detailed analysis can be found in the paper [6]. Further Abaqus-based Rx-FEM solution module will be applied to more challenge bolted composite joint cases such as with the presence of multiple parts contact.

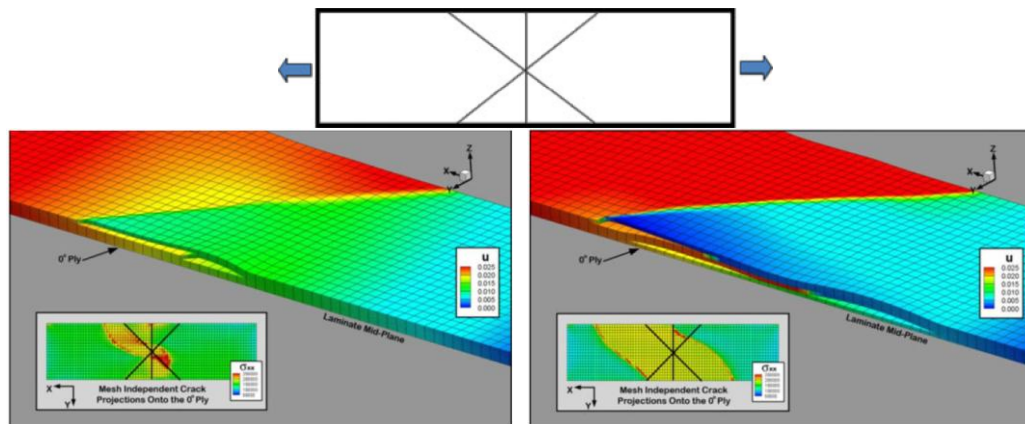


Figure 11. Quasi-isotropic laminate under tension simulated with three pre-existing cracks.

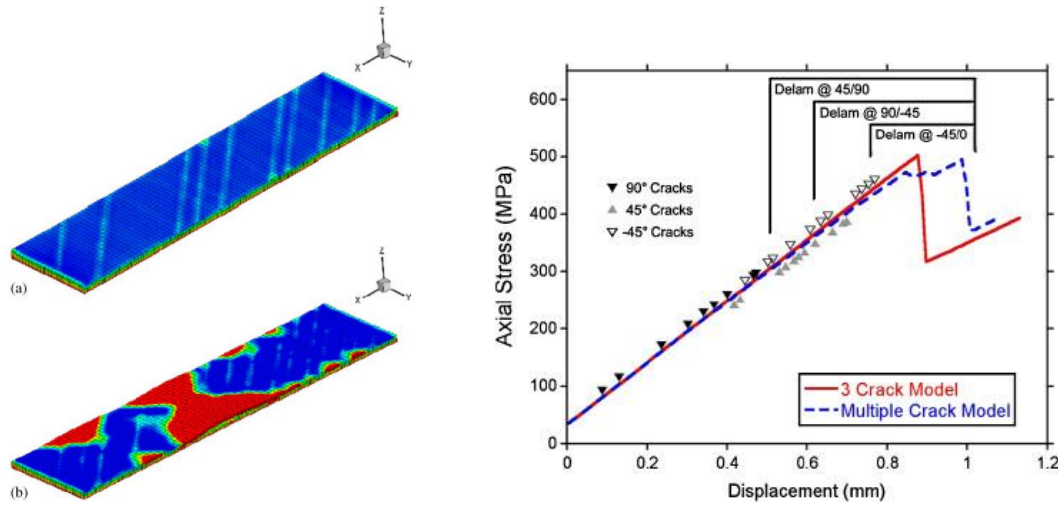


Figure 12. Multiple matrix cracks effect and the stress-displacement curve.

4.3 Fracture parameter extraction for Mode I crack

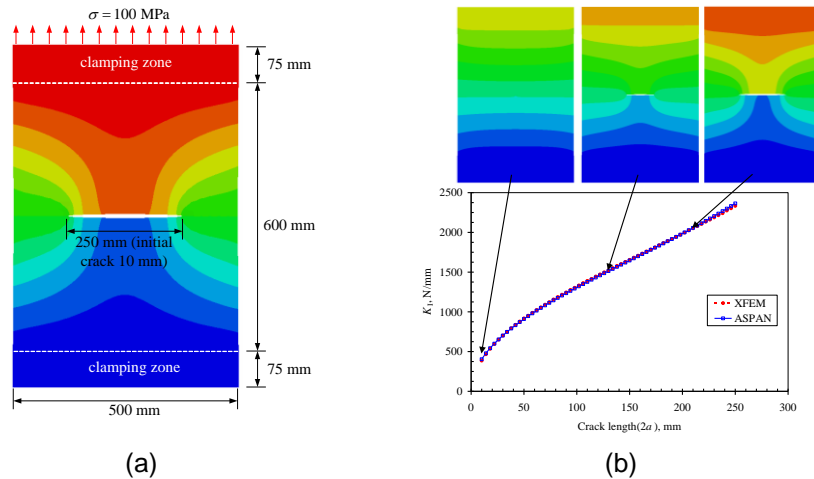


Figure 13. Mode I crack simulation: (a) Geometry and boundary conditions; (b) stress intensity factor evolution with crack length.

This example is used to examine the validity of the phantom paired X-FEM and the reliability of extraction of the fracture parameter using the spring model. As shown in Fig. 13 (a), a clamped plate has its initial crack length of 10 mm subjected to an applied Mode I loading of 100 MPa. The displacement distribution at the crack length of 250 mm is shown in Fig. 13(a). Since the initial crack length is very small compared to the structure dimensions (Figure 13 (b)), the theoretical

solution for the stress intensity factor is given by 396 N/mm which is almost identical to our numerical simulation results. Further, the stress intensity factor vs the crack length curve (K(a)) predicted from our phantom paired X-FEM solution module is almost identical to the ASAPN [8] results (Figure 13 (b)).

4.4 Fatigue delamination prediction of a filled-hole laminated plate subjected to a bypass loading

Fig. 14 shows a filled-hole laminated plate subjected to a bypass loading. To reduce the computational effort during this capability demonstration, we consider the inter-ply delamination failure mode without including the matrix cracking. The delamination zone demonstrates three characteristics clearly: (1) the delamination front can evolve arbitrarily without dependence on the mesh; (2) the delamination pattern has shown generally in-plane symmetric despite that the model is not strictly symmetric. The main reason is that the delamination is mainly driven by the inter-ply shear. For each ply the displacement field is not symmetric but relative displacement trend between the 45° plies and -45° plies are close to the in-plane symmetric condition; (3) the delamination front propagation direction is affected by loading conditions and fiber orientation. The two main branches are both located in the left part due to the presence of the pin load in this area. And the delamination front advances in 45° and -45° direction approximately, which are along the fiber directions.

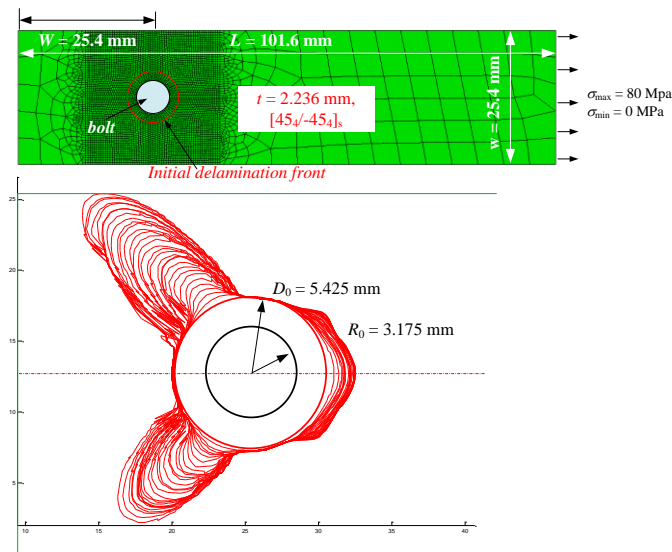
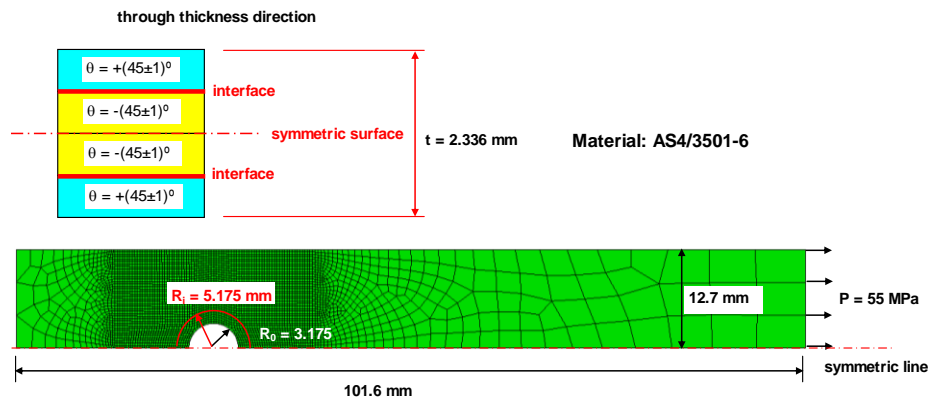


Figure 14. Symmetric delamination zone within [45₄/-45₄]_s laminate.

After the nominal analysis shown above, a parametric study is performed by creating 27 cases with the perturbation of 3 variables. These 27 cases are created by changing three variables via a

full factorial design: the fatigue parameter C in the Paris law (taking values $3.13\text{e-}8$, $3.76\text{e-}8$ and $4.10\text{e-}8$), initial delamination ring width a_i (2.0, 2.25 and 2.5 mm) and the fiber angle θ (44, 45 and 46 degree). The specimen dimensions and loading conditions are shown in Figure 15 and the material is AS4/3501-6. The symmetric BCs are applied to reduce the computational costs. The detailed descriptions of the all 27 cases are listed in Figure 15. Comparing all the delamination front patterns we can see that the initial delamination ring width a_i does not have a significant effect on the delamination speed while the fiber angle θ does have. The larger the angle is, the faster the delamination grows. The main reason is that in this filled-hole tension model the delamination front is dominantly driven by the mode-II energy release rate. Larger fiber angles result in weaker stiffness and larger displacement, which will contribute to a larger energy release rate.

Among these 27 cases, the delamination zone propagation processes of the slowest case (case4 with $C = 3.13\text{e-}8$, $a_i = 2.25$ mm and $\theta = 44^\circ$) and the fastest case (case21 with $C = 4.10\text{e-}8$, $a_i = 2.0$ mm and $\theta = 46^\circ$) are shown in Figure 16. Both curves show a clear characteristic that there are stable growth patterns during the delamination development. The phenomenon indicates that in the pin load filled-hole laminates the delamination zone area does not expand continuously and smoothly. The delamination zone can stay still for a quite long period of time. This is quite different from the fatigue cracking process commonly observed in metallic materials.



(a) model configuration

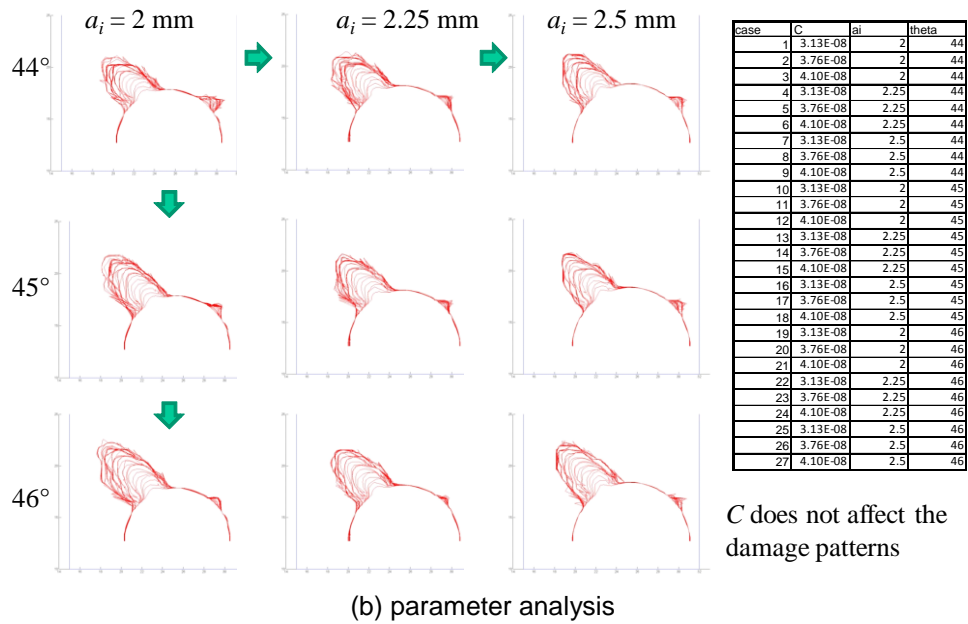


Figure 15. Fatigue delamination evolution.

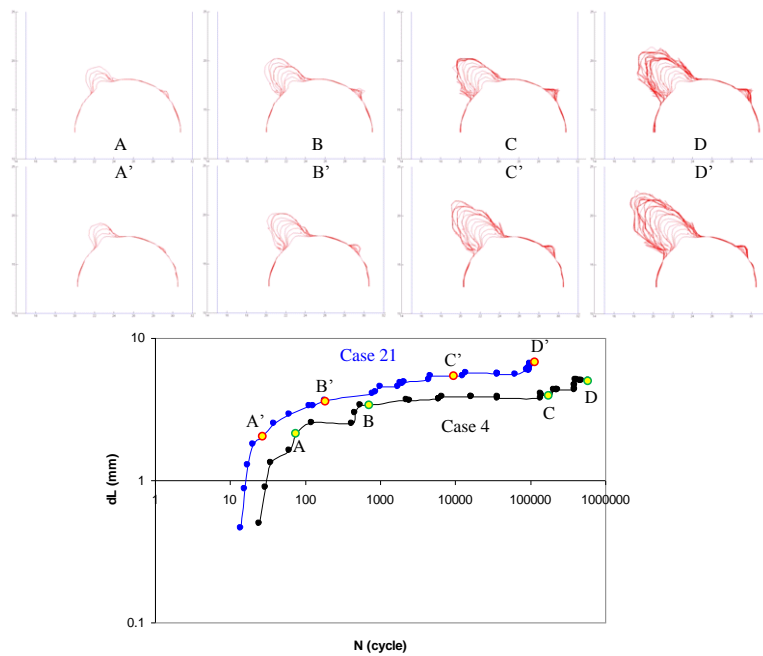


Figure 16. Fatigue delamination processes of selected cases.

5. Conclusions

A high-fidelity discrete crack network (DCN) toolkit for Abaqus has been developed for the residual strength and life prediction of bolted composite joints. A regularized X-FEM (Rx-FEM) and a phantom paired X-FEM have implemented in Abaqus via its UEL to capture the discrete damage evolution and intra and inter ply damage interaction under static and cyclic load, respectively. The use of a smeared crack front representation has shown its attractive feature in maintaining the distribution of the Gauss integration points without element slicing. Initiation and propagation of delaminations between plies as well as intra-ply matrix cracking is controlled by using a mixed-mode cohesive formulation. While the extension of Rx-FEM for the fatigue damage assessment is feasible by bridging the Paris type crack growth law with a cohesive damage evolution law through a calibration process, both the load case and mode mixity dependent fatigue damage accumulation mechanisms can render this calibration process infeasible and impractical.

To circumvent this modeling difficulty, we have implemented the phantom paired X-FEM to retain the sharp crack front representation with smearing. The clear crack front definition enables the direct application of the fracture mechanics driven Paris law to characterize the fatigue crack growth that is fully consistent with the current fatigue testing and damage quantification procedure. By injection of the discrete elastic springs near the fracture process zone, we can extract the range of the strain energy release rates (ΔG) using VCCT along a mesh independent evolving crack front for its fatigue crack growth prediction. Unlike a conventional constitutive model, the use of a linear spring without its softening part can greatly improve the numerical stability and the rate of convergence.

Acknowledgement

The authors gratefully acknowledge the support from the Naval Air Warfare Center, Aircraft Division (Contract No. N68335-09-C-0454 and N68335-11-C-0190) with Dr. Anisur Rahman as program monitor. Partial support was also provided by NASA AAD-2 contract number NNX08AB05A-G and thankfully acknowledged by Swindeman and Iarve.

References

- [1] Iarve, E. V. Mesh independent modeling of cracks by using higher order shape functions. *International Journal for Numerical Methods in Engineering*. 2003, 56:869–882.
- [2] Turon, A., Costa, J., Camanho, P. P., and Davila, C. G. Simulation of Delamination in Composites Under High-Cycle Fatigue. *Composites Part A*, 2007, 38(11):2270-2282.
- [3] Swindeman, M. J. A regularized extended finite element method for modeling the coupled cracking and delamination of composite materials [D]. University of Dayton, Dayton, OH: 2011.
- [4] Camanho, P. P., Davila. Mixed-Mode Decohesion Finite Elements for the Simulation of Delamination in Composite Materials. Report: NASA/TM-2002-211737. 2002 June.

- [5] Camanho, P. P., Turon, A., Davila, C. G., Costa, J.. An Engineering Solution for Mesh Size Effects in the Simulation of Delamination using cohesive zone models. *Engineering Fracture Mechanics*, 2007, 74(10): 1665-682.
- [6] Iarve, E. V., Gurvich, M. R., Mollenhauer, D. H., Rose, C. A., Dávila, C. G.. Mesh-independent matrix cracking and delamination modeling in laminated composites. *International Journal for Numerical Methods in Engineering*, 2007, 88:749–773.
- [7] Hallett, S. R., Jiang, W. G., Khan B, Wisnom , M. R. Modeling the interaction between matrix crack and delamination damage in scaled quasi-isotropic specimens. *Composites Science and Technology*. 2008, 68:80–89.
- [8] Sklyut, H. (2011). Modeling of the advanced hybrid structures using Alcoa Aerospace design tools, presented at the Alcoa/GEM Technical Exchange Meeting on Feb. 15, 2011.